

Nonlocal orbital-free kinetic pressure tensors for the Fermi gas

D. I. Palade*

National Institute of Laser, Plasma and Radiation Physics, P.O. Box MG 36, RO-077125 Măgurele, Bucharest, Romania
and Faculty of Physics, University of Bucharest, Atomistilor 405, RO-077125 Magurele, Romania



(Received 27 August 2018; published 3 December 2018)

A nonlocal density functional for the kinetic pressure tensor of a Fermi gas is derived. The functional is designed to reconcile the quantum hydrodynamic model with the microscopic approaches, both for homogeneous equilibrium and linear dynamic configurations. The derivation paves the way to improving and implementing further time-nonlocal functionals. The present approximation is systematically tested in and beyond the linear regime for the Fermi gas, as well as for some small sodium clusters, proving that it is quantitatively superior to some other density functionals.

DOI: [10.1103/PhysRevB.98.245401](https://doi.org/10.1103/PhysRevB.98.245401)

I. INTRODUCTION

Systems containing (partially) degenerate fermionic species (warm-dense matter [1], nanoparticles [2], metallic clusters [3], semiconductors, thin metal films [4], dense astrophysical objects [5], etc.) have attracted great interest in the past decades, especially due to recent experimental and technological progress. In particular, nanosystems exhibiting quantum plasmonic behavior became one of the paradigms for future nanoelectronic devices [6,7] due to their ability to enhance and localize electromagnetic radiation below the diffraction limit [8].

In general, such systems contain an ionic and one or more fermionic (electrons in metals, electrons and holes in semiconductors) species. Due to their large inertia and localized spatial distribution, ions can be safely considered as being purely classical objects in most scenarios. The fermions, especially at low temperatures and high densities, display strong quantum features following closely the Fermi-Dirac statistic. Naturally, quantum theoretical methods are required to describe the physics behind quantum Fermi systems, both at equilibrium and during their dynamics.

In practice, kinetic (quantum Wigner [9,10]) and microscopic (Hartree-Fock-like [11], time-dependent density functional theory [12]) theories offer high precision to the numerical complexity ratio. Unfortunately, the numerical complexity of microscopic approaches scales with the number of particles, while the kinetic approaches involve (6+1)-dimensional partial differential equations. For example, investigating within density functional theory (DFT) large metal clusters ($\sim 10^{1-2}$ nm and $N \sim 10^{3-4}$ particles) in full three-dimensional (3D) geometry remains a prohibitive numerical task even with the new generation of CPU processors.

In the given context, a simpler model has gained recognition in the past decades, namely the quantum hydrodynamic model (QHD) [4,13]. Although in the literature it appears under different names—(time-dependent-) Thomas-

Fermi [14–16], quantum hydrodynamic theory [17], or quantum fluid theory [18]—it consists mainly of two conservation laws: a continuity equation for the total density of particles $n(\mathbf{r}, t)$ and a momentum equation for the total density of current $\mathbf{j}(\mathbf{r}, t)$ [alternatively, the average velocity field $\mathbf{u}(\mathbf{r}, t) = \mathbf{j}(\mathbf{r}, t)/n(\mathbf{r}, t)$]. The model has been applied with a fair amount of success to a variety of systems: nuclei [19,20], atomic and molecular systems [21], metallic clusters [14,16], quantum plasmas [22,23], etc.

Similar to classical hydrodynamics, the QHD lacks a closure relation between the kinetic pressure tensor $\hat{\Pi}(\mathbf{r}, t)$ and the other lower moments of the distribution function: density and current. Within the DFT, in particular through the Runge-Gross theorems [12], it can be shown that this tensor is a unique (exact and unknown) density functional $\hat{\Pi}(\mathbf{r}, t) \equiv \hat{\Pi}[n(\mathbf{r}, t)]$.

The branch of DFT concerned with this universal functional (or with better approximations of it) is known as orbital-free-DFT (OF-DFT) [24] and it dates back to the foundations of quantum physics. Alternatively, OF-DFT deals with functionals for the kinetic energy, which is equal to the trace of the kinetic pressure tensor. Despite being a long-standing problem, most applications of the QHD still use a functional developed almost a century ago, namely the Thomas-Fermi (-Bohm) approximation (also known as Thomas-Fermi-von Weizsacker [25]):

$$\hat{\Pi}[n] = P_{\text{TF}}[n]\hat{1} - \lambda \frac{\hbar^2}{4m^2} n \nabla \otimes \nabla \ln n, \quad (1)$$

with $P_{\text{TF}}[n_0] = 2E_F[n_0]n_0/5m$ the Thomas-Fermi pressure, $\hat{1}$ the identity tensor, while the second term is a reformulation of the Bohm potential [26], which we shall refer to as macroscopic Bohm pressure. Historically, the λ constant spanned the [0,1] interval. It has been emphasized [15,27] and generally accepted that $\lambda = 1$ for bosonic and $\lambda = 1/9$ for fermionic systems (in three dimensions at $T = 0$ K). A detailed discussion on this matter will be presented throughout this work.

The TF-Bohm approximation belongs to a more general scheme called gradient expansion [28]. Being derived from

*dragos.palade@infpr.ro

the microscopic equilibrium of the homogeneous electron gas (HEG), all these schemes are valid only for the nearly free stationary Fermi gas. Trying to recreate simple dynamic phenomena such as the propagation of an electrostatic wave through a HEG results in the impossibility of TF-Bohm to reproduce (within the QHD) even the dispersion relation in the long-wavelength limit [29]. The previous example hides a very serious pathology: the kinetic/microscopic dynamic behavior of fermionic systems is not captured by the functional (1). From this point of view, the limitations of QHD are surprisingly rarely brought into attention [17,29–31]. The general recipe is to use the approximation (1) with $\lambda = 1/9$ for equilibrium configurations, while in the linear regime the functional is modified to

$$\left(\frac{\delta \hat{\Pi}}{\delta n}\right) = \frac{9}{5} \left(\frac{\delta P_{\text{TF}}[n]}{\delta n}\right) + \lambda \left(\frac{\delta \hat{\Pi}_B[n]}{\delta n}\right),$$

with $\lambda = 1$. This scheme is designed to work only in the limit of high frequency and short wavelengths, its mathematical inconsistency being undeniable evidence that TF-Bohm (and its extensions [28]) are invalid during dynamics. Given these limitations, there should be serious doubts regarding the results of TF-Bohm applications in fully nonlinear regimes dominated by wave-mixing on a wide spectrum of frequencies and wave numbers [22,32,33].

One of the first solutions [34,35] to the inaccuracy of the TF-Bohm functional was designed for the equilibrium configurations of metallic and semiconductor systems. The main proposal was that a density functional should have a nonlocal character in space in order to reproduce the static linear-response function. Recently [17,36], the idea has been extended, stressing that a density functional for the free energy of an electron gas should reproduce within QHD the dynamic linear-response function [Lindhard, random phase approximation (RPA) polarization function].

There is another class of state-of-the-art functionals capable of solving at some level the above-mentioned problem. Comparison with these functionals is not made in the present work since they are either designed solely for the linear regime [37,38] or they are current-density functionals that need a phenomenological parameter [39–41]. Moreover, most of them [40,41] do not account properly for the wave-number dependence of the functionals.

The functionals derived in [17,36] are designed to reconcile *linearized* QHD with the kinetics of an electron gas in asymptotic spectral regions, low ($\omega \ll \hbar k^2/m$) or high ($\omega \gg \hbar k^2/m$) frequency, and they include nonzero temperature effects. At $T = 0$ K they read $\hat{\Pi}_{\alpha,\lambda}^0[n] = \alpha \hat{\Pi}_{\text{TF}}[n] + \lambda \hat{\Pi}_B[n]$, where

$$(\alpha, \beta) = \begin{cases} (1, \frac{1}{9}) & \text{for } \omega \ll \hbar k^2/2m, k \ll k_F, \\ (\frac{3}{5}, 1) & \text{for } \omega \ll \hbar k^2/2m, k \gg k_F, \\ (\frac{9}{5}, 1) & \text{for } \omega \gg \hbar k^2/2m. \end{cases}$$

Their most important feature is the analytical simplicity, which passes as facility in numerical implementation. More importantly, the lack of a unified expression over all spectral regions makes these functionals useless for physical scenarios in which high- and low-frequency modes coexist during dynamics on a wide range of wavelengths [32,33]. This is almost always the case for systems relevant to nanoplasmonics in

nonlinear regimes when high-frequency electrostatic waves are present simultaneously with low-frequency ion dynamics and, sometimes, short-wavelength density oscillations. Finally, there are situations when either the velocity field has rotational components [$\nabla \times \mathbf{u}(\mathbf{r}, t) \neq 0$], or the assumption that $\nabla \cdot \hat{\Pi}[n] = n \nabla(\delta T[n]/\delta n)$, where $T[n]$ is the kinetic energy functional, is not true, therefore invalidating a *standard* [14,16,17,29] field theoretical description. For these reasons, the goal of the present work is to construct a time-nonlocal kinetic pressure density functional (KPDF) that can reproduce concurrently the equilibrium as well as the dynamical linear configurations of a Fermi gas.

The paper is organized as follows: in Sec. II the problem is posed in the contexts of TD-DFT and quantum Wigner equation. The form of the KPDF is motivated from microscopic analysis, and, imposing the associated constraints for equilibrium and linear response, it is explicitly derived. Through a reasonable approximation, the time-nonlocality of the functional is reformulated as a wavelike equation. In Sec. III the validity of the proposed approximation is investigated from a spectral perspective. Extensive comparisons between the KPDF and the microscopic results are performed for the dynamics of a Fermi gas. Finally, realistic small sodium clusters are simulated to establish the qualitative advantages of the KPDF over existing approximations.

II. THEORY

A. Framework

Let us consider an N -body fermionic system. For simplicity, relativistic, temperature, spin, or magnetic effects are neglected. Although not involved in the derivation of the functional, a two-body interaction (e.g., Coulomb) is allowed in addition to an external potential v_{ext} . The microscopic description offered by TD-DFT [12] assigns to each particle a pseudo-orbital $\psi_k(\mathbf{r}, t)$, $\forall k = 1, N$, which obeys the Kohn-Sham (KS) equations:

$$i\hbar \partial_t |\psi_k\rangle = \hat{H} |\psi_k\rangle, \\ \hat{H} = \frac{\hat{p}^2}{2m} + \hat{v}_{\text{eff}}, \quad (2)$$

where \hat{H} is the single-particle Hamiltonian operator, m is the fermionic mass, while v_{eff} is the effective potential, which, aside from the external potential, includes a mean-field interaction and an exchange-correlation term [42] $v_{\text{eff}} = v_{\text{ext}} + v_{\text{mf}} + v_{\text{xc}}$. The ground state is subject to an eigenvalue problem: $\varepsilon_k |\psi_k^0\rangle = \hat{H}_0 |\psi_k^0\rangle$.

An alternative description can be rendered either starting from the N -body quantum Liouville equation all the way through a BBGKY hierarchy [43], or by defining the single-particle density operator from the KS orbitals $\hat{\rho} = \sum_k p_k |\psi_k\rangle \langle \psi_k|$. Both ways deliver the so called quantum Wigner equation [9,10] for $\hat{\rho}$:

$$i\hbar \partial_t \hat{\rho} = [\hat{H}, \hat{\rho}]. \quad (3)$$

Within the position representation, one can define the hydrodynamic quantities as follows: total density of particles,

$$n(\mathbf{r}, t) = \sum_k p_k |\psi_k(\mathbf{r}, t)|^2 = \lim_{\mathbf{r}' \rightarrow \mathbf{r}} \rho(\mathbf{r}, \mathbf{r}', t),$$

total current density,

$$\mathbf{j}(\mathbf{r}, t) = \sum_k p_k \mathbf{j}_k(\mathbf{r}, t) = \frac{\hbar}{2mi} \lim_{\mathbf{r}' \rightarrow \mathbf{r}} (\nabla_{\mathbf{r}} - \nabla_{\mathbf{r}'}) \rho(\mathbf{r}, \mathbf{r}', t),$$

and the kinetic pressure tensor $\hat{\Pi}(\mathbf{r}, t)$,

$$\begin{aligned} \hat{\Pi}_{\text{tot}}(\mathbf{r}, t) &= -\frac{\hbar^2}{4m^2} \sum_k p_k n_k \nabla \otimes \nabla \ln n_k + \sum_k p_k \frac{\mathbf{j}_k \otimes \mathbf{j}_k}{n_k} \\ &= -\frac{\hbar^2}{4m^2} \lim_{\mathbf{r}' \rightarrow \mathbf{r}} (\nabla_{\mathbf{r}} - \nabla_{\mathbf{r}'}) \otimes (\nabla_{\mathbf{r}} - \nabla_{\mathbf{r}'}) \rho(\mathbf{r}, \mathbf{r}', t), \end{aligned} \quad (4)$$

with $n_k = |\psi_k|^2$ the single-particle density and $\mathbf{j}_k = \hbar/2mi(\psi_k^* \nabla \psi_k - \psi_k \nabla \psi_k^*)$ the single-particle current. Either starting from the microscopic KS Eqs. (2) together with a Madelung representation of orbitals $\psi_k = n_k^{1/2} \exp(iS_k/\hbar)$, or simply by using the Wigner Eq. (3), one can derive [4,18] the quantum hydrodynamic model:

$$\partial_t n + \nabla \cdot \mathbf{j} = 0 \quad (5)$$

$$\partial_t \mathbf{j} + \nabla \cdot \left(\frac{\mathbf{j} \otimes \mathbf{j}}{n} \right) + \frac{n}{m} \nabla v_{\text{eff}} + \nabla \cdot \hat{\Pi} = 0. \quad (6)$$

In the momentum equation, $\hat{\Pi} \equiv \hat{\Pi}_{\text{tot}} - \mathbf{j} \otimes \mathbf{j}/n$ denotes the reduced kinetic pressure tensor, which is exactly the topic of the present paper. The Runge-Gross theorems prescribe [12] that the system (5) and (6) is valid and $\hat{\Pi} \equiv \hat{\Pi}[n]$. For future purposes, let us decompose $\hat{\Pi}_{\text{tot}}$ in the *microscopic Thomas-Fermi pressure* $\hat{\mathcal{P}}_{\text{TF}}$ and the *microscopic Bohm pressure* $\hat{\mathcal{P}}_B$:

$$\hat{\mathcal{P}}_{\text{TF}} = \sum_k n_k \mathbf{u}_k \otimes \mathbf{u}_k, \quad (7)$$

$$\hat{\mathcal{P}}_B = -\frac{\hbar^2}{4m^2} \sum_k n_k \nabla \otimes \nabla \ln n_k, \quad (8)$$

where $\mathbf{u}_k = \mathbf{j}_k/n_k$ is the single-particle velocity field. These definitions are consistent with the historical [44] prescription of the Bohm potential.

B. Two Fermi systems

Let us consider two similar systems \mathcal{S}^1 and \mathcal{S}^2 , both depicting the N -body d -dimensional *homogeneous Fermi gas* ($v_{\text{eff}} = 0$, in the thermodynamic limit $N \rightarrow \infty$): \mathcal{S}^1 with periodic and \mathcal{S}^2 with null Dirichlet boundary conditions on a box of length L . \mathcal{S}^1 describes free particles (continuum fermions) while \mathcal{S}^2 describes fully confined fermions. The microscopic stationary orbitals read

$$\psi_k^{\mathcal{S}^1}(\mathbf{r}, t = 0) = L^{-d/2} e^{-i\mathbf{k} \cdot \mathbf{r}},$$

$$\psi_k^{\mathcal{S}^2}(\mathbf{r}, t = 0) = (L/2)^{-d/2} \prod_{j=1}^d \sin(k_j x_j),$$

with $\mathbf{k} = 2\pi/L\mathbf{n}$. By means of the Madelung representation, in \mathcal{S}^1 : $n_k(\mathbf{r}, t) = L^{-d/2}$ and $S_k(\mathbf{r}, t) = \mathbf{k} \cdot \mathbf{r}$, while in \mathcal{S}^2 : $n_k(\mathbf{r}, t) = (L/2)^{-d} \sin(k_j x_j)^2$ and $S_k(\mathbf{r}, t) = 0$. This can be interpreted as follows: in \mathcal{S}^1 the densities n_k have bosonic behavior (the same values $\forall k$) while the phases S_k have

TABLE I. Macroscopic quantities and microscopic pressures for the systems $\mathcal{S}^{1,2}$ at homogeneous equilibrium and during linear dynamics.

| | \mathcal{S}^1 | \mathcal{S}^2 |
|---|--|---|
| $n(\mathbf{r}, t = 0)$ | n_0 | n_0 |
| $\mathbf{j}(\mathbf{r}, t = 0)$ | 0 | 0 |
| $\hat{\Pi}(\mathbf{r}, t = 0)$ | $P_{\text{TF}}[n_0] \hat{1}$ | $P_{\text{TF}}[n_0] \hat{1}$ |
| $\hat{\mathcal{P}}_{\text{TF}}(\mathbf{r}, t = 0)$ | $P_{\text{TF}}[n_0] \hat{1}$ | 0 |
| $\hat{\mathcal{P}}_B(\mathbf{r}, t = 0)$ | 0 | $P_{\text{TF}}[n_0] \hat{1}$ |
| $\delta \hat{\Pi}(\mathbf{r}, t)$ | $\delta \hat{\Pi}(\mathbf{r}, t)$ | $\delta \hat{\Pi}(\mathbf{r}, t)$ |
| $\delta \hat{\mathcal{P}}_B(\mathbf{r}, t)$ | $-\frac{\hbar^2}{4m^2} \nabla \otimes \nabla \delta n$ | $-\frac{\hbar^2}{4m^2} \nabla \otimes \nabla \delta n + \text{other}$ |
| $\delta \hat{\mathcal{P}}_{\text{TF}}(\mathbf{r}, t)$ | $\neq 0$ | 0 |

fermionic behavior (uniform distribution). The converse is true in \mathcal{S}^2 .

All macroscopic quantities, both at equilibrium as well as in the linear regime [under the influence of a small effective potential $\delta v_{\text{eff}}(\mathbf{r}, t)$], can be computed analytically. Table I shows, as completely as possible, these results [$P_{\text{TF}} = 2E_F[n_0]n_0/5m$, the Fermi energy $E_F = \hbar^2 k_F^2/2m$, and the Fermi wave vector $k_F = (3\pi^2 n_0)^{1/3}$].

From a macroscopic perspective, both systems appear to be identical. Nonetheless, upon investigating the microscopic pressures at equilibrium, one can conclude that the macroscopic Thomas-Fermi pressure $\hat{\Pi}_{\text{TF}}[n] = P_{\text{TF}}[n] \hat{1}$ is universal, whereas its nature is related to the fermionic nature of the system: in \mathcal{S}^1 the fermionic character is exhibited by phases (velocities), therefore the microscopic TF reproduces the whole macroscopic TF. In \mathcal{S}^2 the converse is true, with the macroscopic TF being reproduced by the microscopic Bohm. The presence of a macroscopic Bohm pressure $\hat{\Pi}_B = -\hbar^2/4m^2 n \nabla \otimes \nabla \ln n$ at equilibrium can be assumed since the density is uniform and gives null contribution.

Within linear dynamics, the universality of the macroscopic Bohm term $\hat{\Pi}_B$ with a prefactor $\lambda = 1$ that is spectrally independent is suggested by the presence of $-\hbar^2/4m^2 \nabla \otimes \nabla \delta n$ for both systems. Moreover, the deviations of $\hat{\Pi}$ from a TF-Bohm functional cannot be assigned only to the microscopic Bohm term.

In general cases, expanding in Eqs. (7) and (8) the velocities and the densities around their average $\mathbf{u}_k = \mathbf{u}'_k + \mathbf{u}$, $n_k = n/N + n'_k$ yields

$$\hat{\mathcal{P}}_{\text{TF}} = \frac{\mathbf{j} \otimes \mathbf{j}}{n} + \hat{\mathcal{P}}'_{\text{TF}},$$

$$\hat{\mathcal{P}}_B = \hat{\Pi}_B[n] + \hat{\mathcal{P}}'_B,$$

$$\hat{\mathcal{P}}'_{\text{TF}} + \hat{\mathcal{P}}'_B = \hat{\Pi}'_{\text{TF}}[n] + \hat{\Pi}'_{\text{NL}}[n].$$

This decomposition underlines the fact that the advection pressure $\mathbf{j} \otimes \mathbf{j}/n$ and $\hat{\Pi}_B$ are zero-order average terms that should be universal. The macroscopic TF pressure is a consequence of the fermionic character encoded in both microscopic TF and Bohm terms. The residue up to the total real pressure tensor is denoted as $\Pi_{\text{NL}} = \hat{\Pi} - \hat{\Pi}_{\text{TF}} - \hat{\Pi}_B$ and will be investigated later. It must be emphasized that its origin is also the fermionic character of the system and the coupling between \mathcal{P}_{TF} and \mathcal{P}_B .

TABLE II. Asymptotic expansions for the Lindhard function and the LRF reproduced with $\hat{\Pi}_{\alpha,\lambda}^0$ functionals.

| | A | $\chi^{\alpha,\lambda}/A$ | χ^L/A |
|-----------------------------|--------------------------------|--|--|
| $\omega = 0, k \ll k_F$ | $-\frac{3mn_0}{\hbar^2 k_F^2}$ | $\frac{1}{\alpha} - \frac{3\lambda k^2}{4\alpha^2 k_F^2}$ | $1 - \frac{\lambda k^2}{12k_F^2}$ |
| $\omega = 0, k \gg k_F$ | $-\frac{4mn_0}{\hbar^2 k^2}$ | $\frac{1}{\lambda} - \frac{4\alpha k_F^2}{3k^2 \lambda^2}$ | $1 + \frac{4k_F^2}{5k^2}$ |
| $\omega \rightarrow \infty$ | $\frac{k^2 n_0}{m\omega^2}$ | $1 + \frac{\alpha k^2 k_F^2 \hbar^2}{3m^2 \omega^2} + \frac{\lambda k^4 \hbar^2}{4m^2 \omega^2}$ | $1 + \frac{3k^2 k_F^2 \hbar^2}{5m^2 \omega^2} + \frac{k^4 \hbar^2}{4m^2 \omega^2}$ |

C. Pressure tensors and linear response

Linearizing around homogeneous equilibrium $n(\mathbf{r}, t) = n_0 + \delta n(\mathbf{r}, t)$, $\mathbf{j}(\mathbf{r}, t) = 0 + \delta \mathbf{j}(\mathbf{r}, t)$, and $\hat{\Pi}(\mathbf{r}, t) = \hat{\Pi}_0 + \delta \hat{\Pi}(\mathbf{r}, t)$ in the QHD (5) and (6) and taking the space-time Fourier transform, \mathfrak{F} , an *exact* equation for the functional derivative of the pressure can be found:

$$\mathfrak{F}\left(\frac{\delta \hat{\Pi}^{kk}(r, t)}{\delta n(r', t')}\right) = \frac{\delta \Pi^{kk}}{\delta n}(\omega, k) = \frac{\omega^2}{k^2} - \frac{n_0}{m\chi(\omega, k)}, \quad (9)$$

where $\chi(r, r', \omega) = \delta n / \delta v_{\text{eff}}$ is the linear-response (polarization) function (LRF), and the superscript kk indicates the $\mathbf{e}_k \times \mathbf{e}_k$ component of the tensor. For the fermionic gas, χ can be analytically computed as a Lindhard function [45]:

$$\chi^L(\omega, k) = \pm \frac{dn_0}{2E_F} \frac{k_F}{k} \Psi_d\left(\frac{\omega + i\eta}{kv_F} \mp \frac{k}{2k_F}\right),$$

$$\Psi_d(z) = \int_0^1 dx x^{d-1} \int d\Omega_d / \Omega_d [z - x \cos(\theta)]^{-1},$$

$$\Psi_3(z) = \frac{z}{2} + \frac{1-z^2}{4} \log \frac{z+1}{z-1}.$$

Equation (9) asserts for any functional $\hat{\Pi}[n]$ a LRF χ^Π . In Table II we compare the asymptotic χ^L and the LRF associated with $\hat{\Pi}_{\alpha,\lambda}^0$. By direct comparison, the coefficients found in [17] can be seen to be valid.

Ultimately it must be emphasized that in the literature [17,36], first-order gradient corrections of the OF functionals are called Bohm due to their resemblance with the original Bohm potential. In the present work, it is shown that, beyond terminology, such corrections (consequently, the values of λ) do not originate from *microscopic Bohm* but rather from the coupling between microscopic Bohm and microscopic TF.

D. A nonlocal functional

The standard philosophy of orbital-free-DFT is based on the local density approximation (LDA): a functional that reproduces exactly the pressure (through a set of constraints) for a specific system (usually homogeneous) is found, and its closed form is generalized to any density $n(\mathbf{r}, t)$ (the LDA limit). The present functional will be derived imposing the above-mentioned equilibrium and linear dynamics constraints (already used in the literature [17]):

$$\hat{\Pi}[n_0] = P_{\text{TF}}[n_0] \hat{1}, \quad n_0 = \text{const}, \quad (10)$$

$$\frac{\delta \Pi^{kk}}{\delta n}(\omega, k) = \frac{\omega^2}{k^2} - \frac{n_0}{m\chi^L(\omega, k)}. \quad (11)$$

Note that the constraint (11) does not include properly [17] the exchange-correlation effects, but it relies on the presence of a LDA exchange-correlation potential in the effective potential used in the QHD equations (6). In Sec. II B it has been suggested based on microscopic considerations that any KPDP can be decomposed in a zero-order macroscopic Bohm and a first order, fermionic, macroscopic TF pressure along with another unknown term. This decomposition is proven in detail from a kinetic perspective in Appendix A 1. Taking into account the analytic form of the Lindhard function in the Fourier domain for the condition (11), it becomes obvious that $\delta \hat{\Pi}(r, t) / \delta n(r', t')$ must be nonlocal in space and time. The locality of the TF-Bohm terms implies time-nonlocality of the residual term $\hat{\Pi}_{\text{NL}}[n]$. By dimensional analysis (Appendix A 1),

$$\hat{\Pi}[n] = -\frac{\hbar^2}{4m^2} n \nabla \otimes \nabla \ln n + P_{\text{TF}}[n] \hat{1} + \hat{\Pi}_{\text{NL}}[n],$$

$$\hat{\Pi}_{\text{NL}} = \frac{\hbar^2}{2m^2} \int dx' \delta(x - x') (\nabla_{\mathbf{r}} \otimes \nabla_{\mathbf{r}'} + \nabla_{\mathbf{r}'} \otimes \nabla_{\mathbf{r}}) \tilde{\rho}(x, x'),$$

$$\tilde{\rho}(x, x') = \int dy dy' n^{1/2}(y) O(x, y, x', y'; n(x), n(x')) n^{1/2}(y),$$

where $x = (\mathbf{r}, t)$, $y = (\mathbf{r}', t')$, and the double density-dependent kernel $O(x, y, x', y'; n_1, n_2)$ has been introduced. Further detailed calculus is presented in Appendix A 1. Due to translational invariance of the ground-state density $n_0 = \text{const}$, the kernel is assumed invariant, $O(x, y, x', y'; n_0, n_0) \equiv O(x - y, x' - y'; n_0, n_0)$, and the constraints (10) and (11) are worked out within a Fourier representation $O(\xi, \zeta; n_1, n_2)$ with $\xi \equiv (\omega, \mathbf{k})$. The outcome, together with a supplementary ansatz and the LDA limit,

$$O(x, y, x', y'; n(x), n(x')) \equiv \lim_{\substack{n_1 \rightarrow n(x) \\ n_2 \rightarrow n(x')}} O(x, y, x', y'; n_1, n_2),$$

lead us toward the central result of this work:

$$\hat{\Pi}_{\text{NL}}[n] = \int dx' \mathcal{L}(x, x') [n^{1/2}(x) \mathcal{D}(x') + n^{1/2}(x') \mathcal{D}(x)],$$

$$\mathcal{L}(x, x') = \delta(x - x') (\nabla_{\mathbf{r}} \otimes \nabla_{\mathbf{r}'} + \nabla_{\mathbf{r}'} \otimes \nabla_{\mathbf{r}}) (\nabla_{\mathbf{r}} \nabla_{\mathbf{r}'})^{-1},$$

$$\mathcal{D}(x) = \frac{1}{2} \int dy \int d\xi e^{-i\xi(x-y)} \phi(\xi; n(x)) n^{1/2}(y),$$

$$\phi(\xi; n_0) = \frac{\omega^2}{k^2} - \frac{n_0}{m\chi(\omega, k)} - \left(\frac{\delta \Pi_B}{\delta n} + \frac{\delta \Pi_{\text{TF}}}{\delta n} \right)_{n_0}. \quad (12)$$

The functional (12) presents two levels of complexity. First, the operator $\mathcal{L}(x, x')$ involves solving an intricate 6D partial differential equation. This can be overcome either by considering various symmetries of the system or using the free-energy density as a trace of the pressure tensor: $\tau_{\text{NL}}[n] = \text{Tr} \hat{\Pi}_{\text{NL}}[n]$:

$$\hat{\Pi}_{\text{NL}} \approx \tau_{\text{NL}}[n] \nabla \ln n \otimes \nabla \ln n,$$

$$\nabla \cdot \hat{\Pi}_{\text{NL}} \approx \nabla \tau_{\text{NL}}[n].$$

Both choices are consistent with the conditions (10) and (11). The second difficulty is related to the time-nonlocality, which requires convoluting the kernel ϕ with the density at all times. The convolution is partially removed by the causal

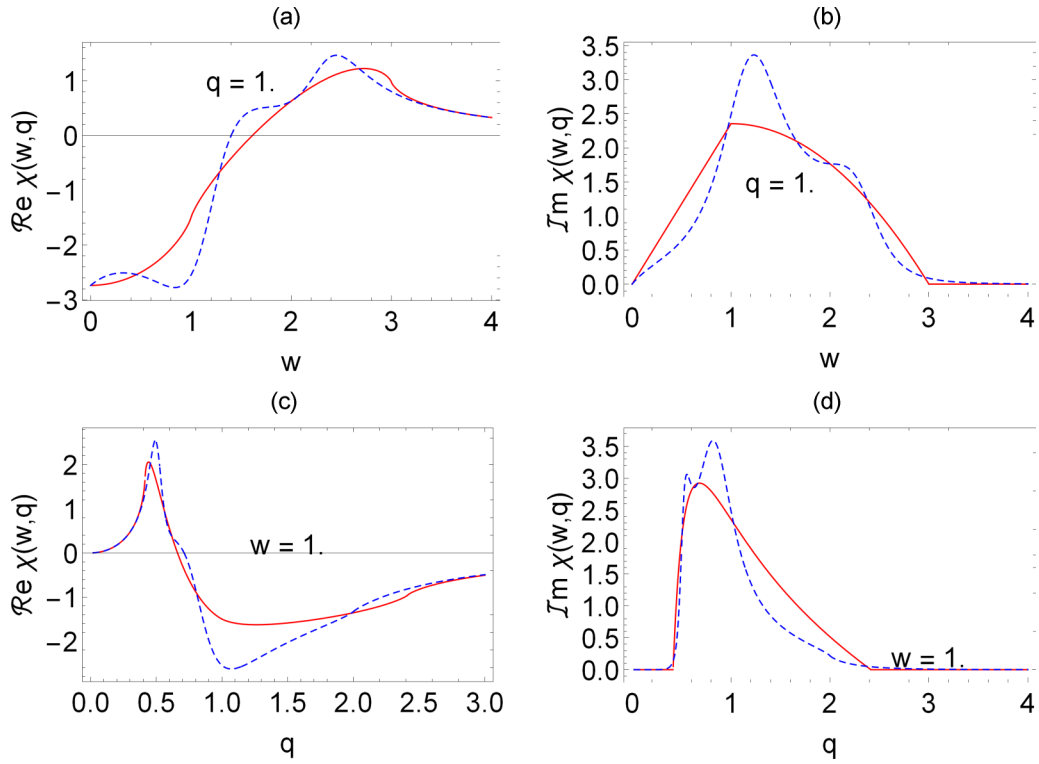


FIG. 1. (a), (c) Real and (b), (d) imaginary parts of the Lindhard function (red) and the approximative LRF χ^{app} (blue, dashed) at $q = 1$ (a), (b) and $w = 1$ (c), (d).

character of the LRF χ^L , which makes \mathcal{D} causal:

$$\mathcal{D}(\mathbf{r}, t) = \frac{1}{2} \int d\mathbf{r}' \int_{-\infty}^t dt' \phi(|\mathbf{r} - \mathbf{r}'|, |t - t'|; n(\mathbf{r}, t)) n(\mathbf{r}', t')^{1/2}. \quad (13)$$

Even though this form can be implemented in principle, it represents a tremendously difficult numerical workload. A workaround this problem is presented.

E. An approximate functional

The formula (13) suggests that $\phi(|\mathbf{r} - \mathbf{r}'|, |t - t'|; n(\mathbf{r}, t))$ can be seen as a propagator, i.e., a Green function, which in turn could be given by an integral equation for \mathcal{D} . On the other hand, local (differential) equations have Green functions that in the Fourier representation can be expressed as rational functions. Motivated by this idea and inspired by Drude-like approximations of the dielectric constant together with the asymptotic behavior of the kernel ϕ , the following approximative form is proposed:

$$\phi^{\text{app}}(\omega, k) \approx \phi_0^\infty \frac{\omega^2 - i\gamma(k)\omega + t_2(k)}{\omega^2 - i\gamma(k)\omega + t_1(k)} \quad (14)$$

designed to reproduce the kernel $\phi(\omega, k)$ exactly at the asymptotic limits $\omega = 0$, $\omega \rightarrow \infty$ and the midline inside the particle-hole continuum, i.e., $\omega = \hbar^2 k^2 / 2m + \hbar k / m$. The presence of the imaginary term has a threefold importance: it helps reproduce the exact kernel, it models the dissipative phenomena (Landau damping), and it makes the kernel analytical in the complex plane. The last property implies causality and,

consequently, the validity of the F-sum rule:

$$-\frac{2}{\pi} \int_{-\infty}^{\infty} \omega \mathcal{I}m[\chi^{\text{app}}](\omega, q) = \frac{n_0 q^2}{m}.$$

Skipping the details of the calculus presented in Appendix A2, the approximation (14) allows us to write a wavelike equation for \mathcal{D} with nonconstant coefficients and source:

$$[\partial_{t,t} - \hat{\gamma} \partial_t - \hat{t}_1] \mathcal{D} = \frac{4\hbar^2 k_F^2}{15m^2} [\partial_{t,t} - \hat{\gamma} \partial_t - \hat{t}_2] n^{1/2}, \quad (15)$$

where the operators $\hat{\gamma}[n]$, $\hat{t}_1[n]$, and $\hat{t}_2[n]$ and their action on spatial functions are defined in Appendix A2. The term \mathcal{D} is now an approximation for the one prescribed by Eq. (13), but the one that should be used in practice as it is much easier to compute numerically thanks to its local-in-time nature.

Through the identity $\tau[n] = \text{Tr} \hat{\Pi}[n]$ one can develop a field-theoretical QHD [15–17] where the approximation $\nabla \cdot \hat{\Pi}[n] = n \nabla(\delta T[n] / \delta n)$ holds and the kinetic density functional

$$T[n] = 2 \int dx dx' \delta(t - t') n(x)^{1/2} \phi(x - x'; n(x)) n(x')^{1/2}.$$

At this point, let us collect the full prescription of the functional (referred to from now on as KPFD), which will always be used in practice instead of the one given in Eq. (13) as it is orders of magnitude easier to implement numerically:

$$\hat{\Pi}[n] = \frac{\hbar^2 n k_F^2}{5m^2} \hat{1} - \frac{\hbar^2}{4m^2} n \nabla \otimes \nabla \ln n + \hat{\Pi}_{\text{NL}}[n],$$

$$\hat{\Pi}_{\text{NL}}[n] = \int dx' \mathcal{L}(x, x') [n^{1/2}(x) \mathcal{D}(x') + n^{1/2}(x') \mathcal{D}(x)],$$

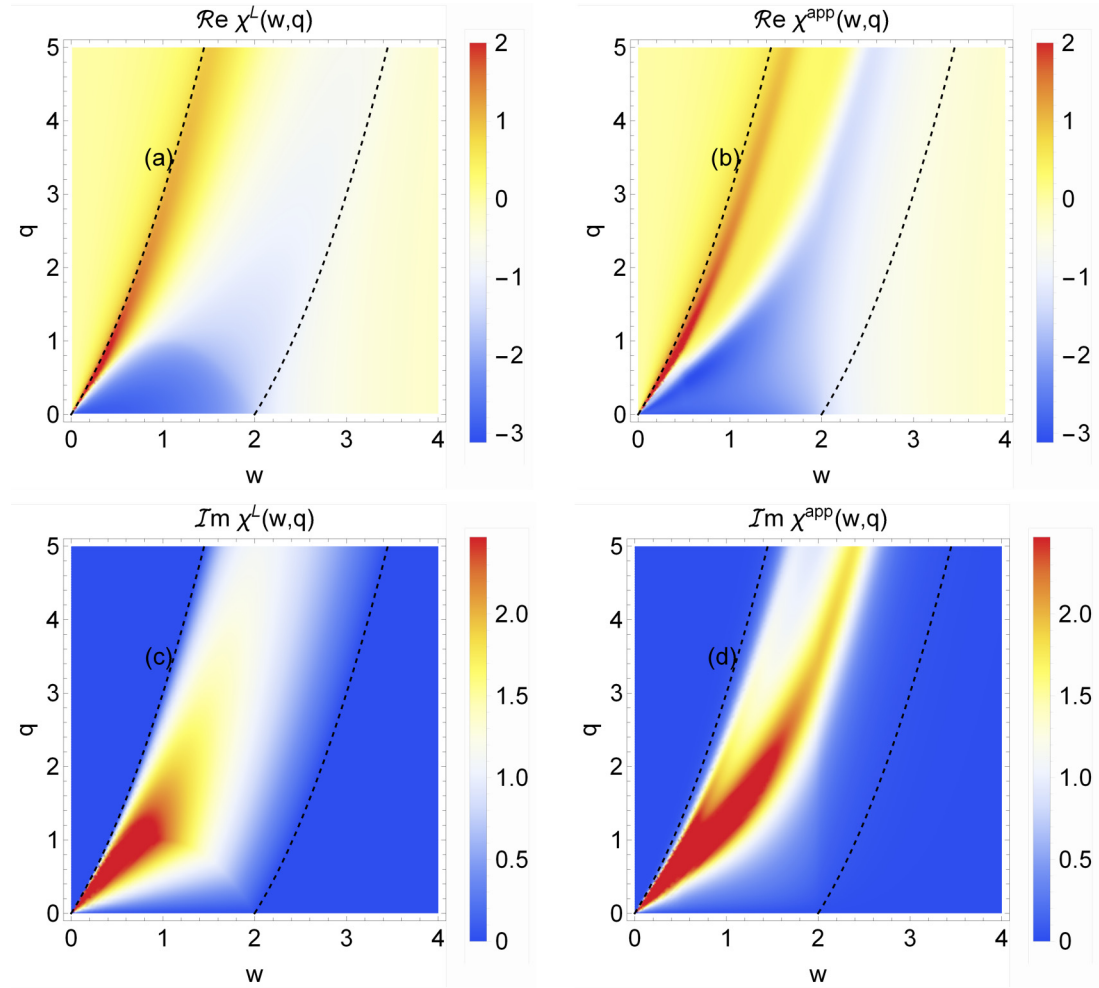


FIG. 2. (a), (b) Real and (c), (d) imaginary parts of the Lindhard function (a), (c) and the approximative LRF χ^{app} (b), (d).

$$\mathcal{L}(x, x') = \delta(x - x')(\nabla_{\mathbf{r}} \otimes \nabla_{\mathbf{r}'} + \nabla_{\mathbf{r}'} \otimes \nabla_{\mathbf{r}})(\nabla_{\mathbf{r}} \nabla_{\mathbf{r}'})^{-1},$$

$$(\partial_{t,t} - \hat{v} \partial_t - \hat{t}_1) \mathcal{D} = \frac{4\hbar^2 k_F^2}{15m^2} (\partial_{t,t} - \hat{v} \partial_t - \hat{t}_2) n^{1/2},$$

$$\nabla \cdot \hat{\Gamma}_{\text{NL}}[n] \approx 4\nabla(n^{1/2} \mathcal{D}).$$

III. RESULTS

A. Accuracy of the approximative kernel

Before testing the validity and the improvements brought about by the KPDF for realistic systems, it is important to understand what is lost along the approximation (15). The best picture is provided by the comparison between the exact $\chi^L(w, q)$ and the $\chi^{\text{app}}(w, q)$ associated by Eqs. (9) and (14) with \mathcal{D} . From now on, the following scaling will be adopted: $w \equiv m\omega/\hbar k_F^2$, $q \equiv k/k_F$, $\chi \equiv \chi v_F^2$.

Since, by design, the LRF's should agree well asymptotically ($w \gg q^2$ and $w \ll q^2$), in Fig. 1 we plot the real and imaginary parts of $\chi^L(w, q)$ and $\chi^{\text{app}}(w, q)$ at $w = 1$ and $q = 1$, where large discrepancies are expected. The exact profile of χ^L is fairly well interpolated by χ^{app} in between the asymptotics. As a pitfall, a smooth tail appears in the imaginary part of $\chi^{\text{app}}(w, q)$ outside the particle-hole

continuum, indicating a pathological presence of the damping. This behavior is a consequence of the smooth analytic form (14), which cannot reproduce the logarithmic discontinuities of χ^L (its derivatives).

A comprehensive comparison is shown in Fig. 2 for the same quantities as in Fig. 1 but on the whole spectrum (w, q) as a density-plot.

As expected, the approximative KPDF works very well asymptotically, outside the particle-hole continuum defined by $w = \max(q^2 \pm 2q, 0)$. While inside this region errors up to 50% are expected, the trends of the Lindhard function are reproduced. This is expected to lead to good qualitative behavior in realistic simulations. Other approximations of the kernel ϕ compatible with time-locality and capable of reproducing even better the Lindhard function might be designed, but the present work is concerned with the simplest of them as it is the easiest to implement numerically.

B. Extensive Monte Carlo tests

The results shown in Figs. 1 and 2 indicate the levels of accuracy for the approximative KPDF in the linear regime from a spectral perspective. However, in realistic scenarios, the external potential is induced as an initial value quantity simul-

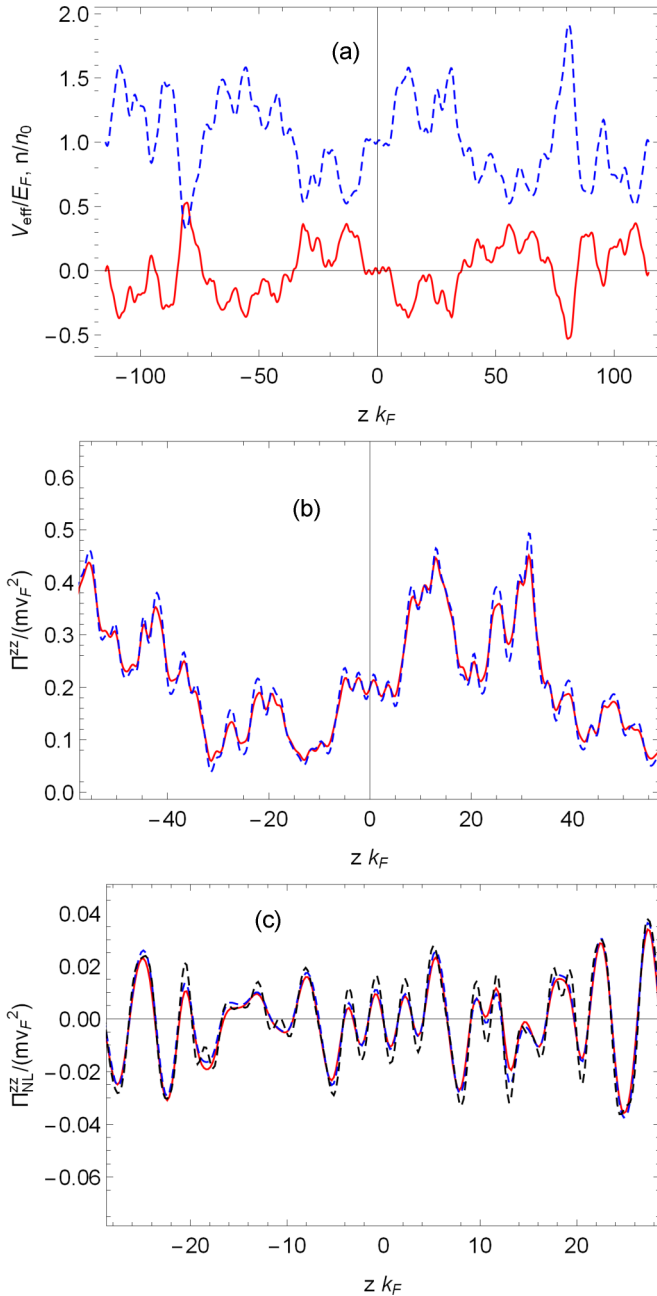


FIG. 3. (a) Generic random potential (red, full line) and the associated ground-state density profile of the Fermi gas (blue, dashed); (b) spatial profile of the z, z component of microscopic pressure (red, full line) and the $\hat{\Pi}_{1,1}^0$ approximation (blue, dashed); (c) the spatial profile for the z, z component of the nonlocal microscopic (red, full line), the KPDF (blue, dashed), and $\hat{\Pi}_{1,1/9}^0$ (black, dashed) pressure.

taneously affecting multiple spectral regions. Even more, one cannot estimate how the second-order mode coupling, which is enabled beyond the purely linear regime, will be reflected in the KPDF. Finally, will the errors from the particle-hole continuum region have only a quantitative impact or also a qualitative one, perhaps leading to unphysical behaviors? To answer all these questions in an exhaustive manner, a simple toy system is used.

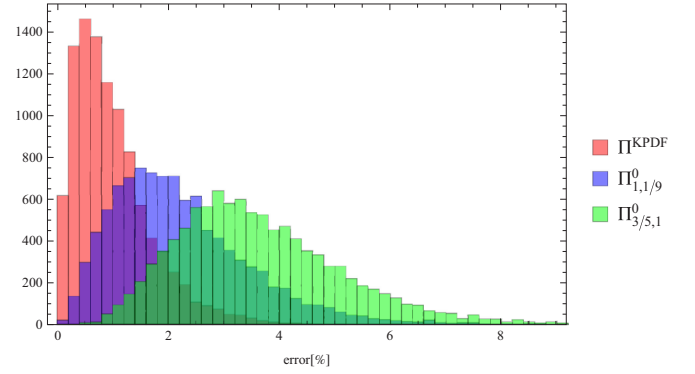


FIG. 4. Distribution of error in the Monte Carlo ensemble of stationary profiles provided by KPDF (red), $\hat{\Pi}_{1,1/9}^0$ (blue), and $\hat{\Pi}_{3/5,1}^0$ (green).

The system is a 3D Fermi gas under spatial periodic boundary conditions. For the stationary regime, the gas is assumed in its ground state under the influence of a static effective potential $v_0(z)$, while for dynamics the system is considered to be found in a homogeneous ground state at $t < 0$ and subjected to an effective potential $v(z, t)$ at $t \geq 0$. The unidirectional dependency on Oz axes is chosen for simplicity, without spoiling the main conclusions of the analysis. The potential $v(z, t)$ supports a Fourier decomposition:

$$v(z, t) = \int d\omega dk A(\omega, k) e^{-i(\omega t - kz)}.$$

Due to translational invariance in the $\mathbf{r}_\perp = (x, y)$ plane, the KS pseudo-orbitals for each particle can be represented as

$$\Psi_{\mathbf{k}}(\mathbf{r}_\perp, z, t) = e^{-i\mathbf{k}_\perp \cdot \mathbf{r}_\perp} e^{-i\frac{\hbar \mathbf{k}_\perp^2}{2m} t} \psi_{k_z}(z, t),$$

with $\mathbf{k} = \mathbf{k}_\perp + \hat{\mathbf{e}}_z k_z$ obeying the KS equations:

$$i\hbar \partial_t \psi_{k_z}(z, t) = \left[-\frac{\hbar^2}{2m} \partial_{zz} + v(z, t) \right] \psi_{k_z}(z, t) \quad (16)$$

at homogeneous stationarity: $\psi_{k_z}(t=0) = \exp^{-ik_z z}$, where $k_F \leq k_z \leq k_F$. The macroscopic quantities can be obtained after averaging over the orthogonal degeneracy \mathbf{k}_\perp :

$$\begin{aligned} n(z, t) &= \frac{3}{4k_F^3} \int_{-k_F}^{k_F} (k_F^2 - k_z^2) |\psi_{k_z}|^2 dk_z, \\ j_z(z, t) &= \frac{3\hbar}{4mk_F^3} \int_{-k_F}^{k_F} (k_F^2 - k_z^2) \text{Im}(\psi_{k_z}^* \partial_z \psi_{k_z}) dk_z, \\ \Pi_{\perp, \perp}(z, t) &= \frac{3\hbar^2}{8m^2 k_F^3} \int_{-k_F}^{k_F} (k_F^2 - k_z^2)^2 |\psi_{k_z}|^2 dk_z, \\ \Pi_{z, z}(z, t) &= \frac{3\hbar^2}{4m^2 k_F^3} \int_{-k_F}^{k_F} (k_F^2 - k_z^2) |\partial_z \psi_{k_z}|^2 dk_z. \end{aligned}$$

Other quantities are $j_\perp = 0$, $\Pi_{\perp, z} = \Pi_{z, \perp} = 0$.

Equation (16) is solved numerically using a pseudospectral method [46] on a uniform 1D grid. Variables and quantities are scaled as follows: density by ground state n_0 , current by $v_F n_0$, pressure by $2n_0 E_F / m$, the potential with E_F , the space variable z with k_F^{-1} , and time by $(E_F / \hbar)^{-1}$. The spatial domain $L = \pi N$ is discretized in 2^{10} equidistant points, while

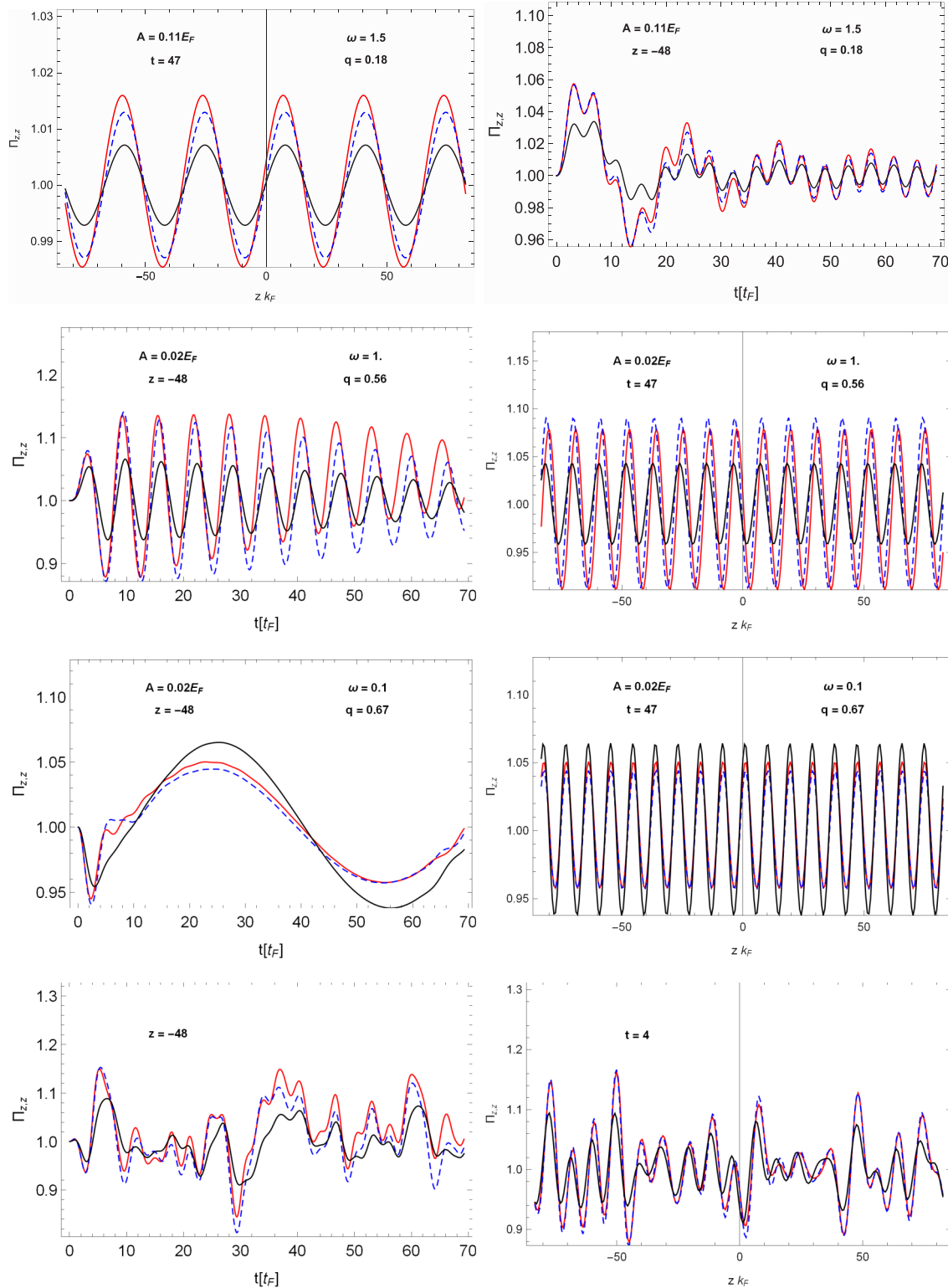


FIG. 5. Temporal (left) and spatial (right) profiles of the pressure at a specific point in space and time, respectively. The profiles are computed via the microscopic method (red, full line), KPDF (blue, dashed), and $\hat{\Pi}_{9/5,1}^0$ (black).

$N = 200$ was chosen to resolve the thermodynamic limit $N \rightarrow \infty$ of a Fermi gas. The temporal evolution is done via an operator-splitting technique with constant time steps $\delta t \approx 10^{-3}$ to ensure reasonable ($\leq 10^{-2}\%$) conservation of total norm, energy, and momentum. Testing the approximative

KPDF is equivalent to comparing $\Pi_{z,z}^{\text{app}}$ against the exact, microscopic $\Pi_{z,z}$, the former being computed from the *exact* density profile obtained from microscopic simulations.

At this point, the purpose is to test the KPDF in complicated scenarios, possibly beyond the linear regime,

and compare it with the more recent functionals $\hat{\Pi}_{\alpha,\lambda}^0$ [17]. This will be achieved considering a Monte Carlo ensemble of effective potentials, each one with a wide spectrum. The amplitudes $A(\omega, k)$ for each potential $v(z, t)$ are randomly generated with a probability $P(A, w, q) \sim \exp[-5|A|^2]\Theta(3 - |w|)/(q^2 + 1)$. With this probability function, the system is forced to go beyond the linear regime, on slow and fast timescales, at short and long wavelengths.

Stationary states are resolved solving Eq. (16) using the imaginary-time method. In Fig. 3(a) we plot a generic potential (red, full line) from the ensemble and the associated total density (blue, dashed). It is found that for ground states, even the TF-Bohm ($\lambda = 1$) provides fairly good agreement with the microscopic pressure, which can be seen in Fig. 3(b). For that, in Fig. 3(c) we compare the nonlocal parts of the pressure profiles (beyond TF-Bohm, $\Pi_{\text{NL}} = \Pi - \Pi_{\text{TF}} - \Pi_{\text{B}}$) computed microscopically (red), with the KPDF (blue) and with $\Pi_{1,1/9}^0$ (black). Such results are generic for the whole ensemble, therefore we proceed to capture its statistics by computing the error in each case (see Fig. 4). The error for an approximate functional is defined as

$$\text{error} = \frac{\int_0^T dt \int_0^L dz |\Pi_{z,z}(z, t) - \Pi_{z,z}^{\text{app}}(z, t)|}{\int_0^T dt \int_0^L |\Pi_{z,z}(z, t)|}$$

Obviously, the time integral will be relevant only for the dynamic case. In the histogram (4) we show the results for the approximative KPDF (red) in comparison with the ones provided by $\hat{\Pi}_{3/5,1}^0$ (green, valid at high wave numbers) and by $\hat{\Pi}_{1,1/9}^0$ (blue, valid at low wave numbers). Although no explanation was found for the γ -like distributions, it is a clear representation of how, qualitatively, the KPDF is on average almost an order of magnitude more precise than $\hat{\Pi}_{\alpha,\lambda}^0$ approximations, yielding also a lower dispersion of the errors.

The dynamic regime is the real test for the approximative nature of the KPDF. For that, another ensemble is generated, only now with frequency-dependent modes. In Fig. 5 we plot the pressure profiles: microscopic (red), the present KPDF (blue, dashed), and $\Pi_{\alpha,1}^0$ (black) for certain spectral modes and at certain time (right) and space (left) points. As expected from the previous analysis, in the asymptotic regions the results are well reproduced. Moreover, in the intermediate area ($w = 1, q = 0.5$), despite somewhat larger quantitative errors, the qualitative trends are closely followed. In the bottom figure, the results of a random potential are presented with the same qualitative/quantitative trends.

As in the stationary case, we chose to gather the ensemble results in a histogram (6) of the errors. In contrast with the ground state, the dynamic regime reveals errors that are one order of magnitude larger (see Fig. 6). For the recent [17] $\hat{\Pi}_{9/5,1}^0, \hat{\Pi}_{1,1/9}^0$ functionals, this can be understood as a consequence of not being able to deal with certain spectral components of the potential. For the KPDF, errors arise mainly from the particle-hole continuum modes as well as from going beyond the linear regime. In particular, the KPDF works better than $\hat{\Pi}_{\alpha,\lambda}^0$ because the former includes (through the $\hat{\gamma}$ operator) the Landau damping, which is essential in dynamical regimes. In a broader sense, the KPDF captures better the microscopic behavior of particle-hole excitations.

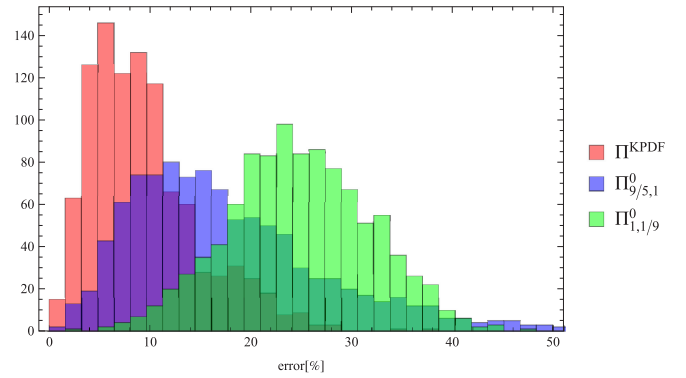


FIG. 6. Distribution of errors in the dynamic Monte Carlo ensemble by KPDF (red), $\hat{\Pi}_{1,1/9}^0$ (green), and $\hat{\Pi}_{9/5,1}^0$ (blue).

C. Testing on metal clusters

In the previous sections, it has been shown that KPDF deals well with a Fermi gas in most spectral cases and slightly above linear dynamics. Still, the agreement is a consequence of working within the thermodynamic limit (a large number of particles). There are many systems of interest, especially to nanoplasmonics, which are finite, lack spatial periodicity, and contain a small number of electrons. All these features might hinder the applicability of the KPDF (in particular, the problem of N -representability [47] connected with the low number of fermions).

To understand what is expected in such scenarios, let us consider as a final test the case of small spherical sodium clusters Na_{20} and Na_{40} . These are a conglomerate of sodium atoms, approximately spherical, in which the valence electrons are known to exhibit special behavior. In particular, they are known to support electrostatic normal modes relevant for the optical spectra known as localized volume and surface plasmons [48]. The ground state and the normal mode dynamics of these systems are resolved both microscopically (solving the LDA Kohn-Sham equations for the valence electrons within the jellium model) and macroscopically (solving the QHD with the KPDF). Details about the jellium model and numerical implementation of KS equations can be found in [48]. In particular, the exchange-correlation potential is introduced through a LDA parametrization [49].

In Fig. 7 we plot the radial profiles of density obtained with KS, KPDF, $\hat{\Pi}_{1,1}^0$, and $\hat{\Pi}_{1,1/9}^0$. As can be seen, the shell effect in the core of the cluster cannot be reproduced by any of the functionals, this being a direct reflection of the representability problem. This remains a major challenge with respect to future improvements that can be brought to any functional. Apart from this core behavior, one can see that both the KPDF and $\Pi_{1,1}^0$ are able to reproduce the exponential density tail (inset of Fig. 7). This feature (the electronic spill-out in general) is of great importance [29,30] in many surface phenomena, such as the static polarizability or the surface plasmon resonance. Again, the KPDF is overall more accurate than any of the other two functionals. Regarding the shell oscillations in density, we expect that they get smaller with the size of the cluster, such that, for large clusters, the system is more Fermi-gas-like, and the errors should be much smaller.

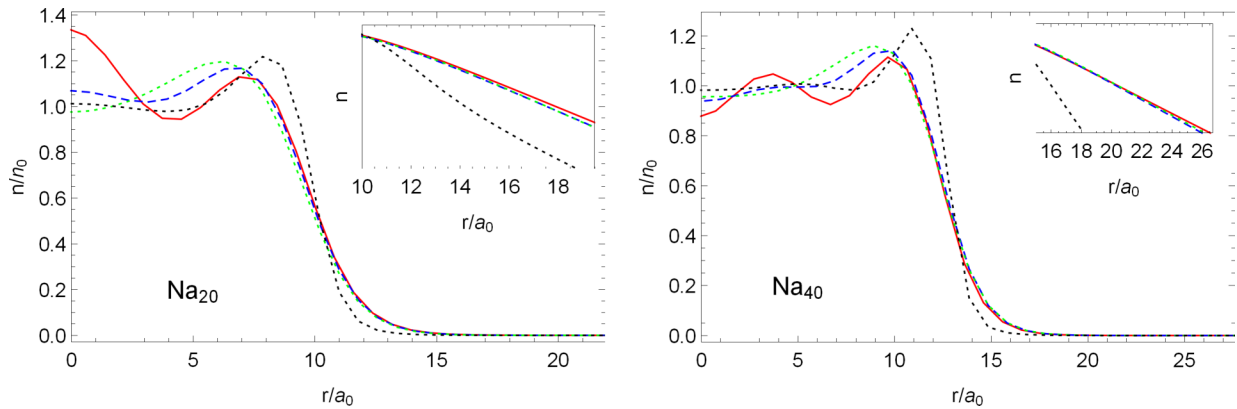


FIG. 7. Ground-state electronic density profiles for Na_{20} (left) and Na_{40} (right) computed with DFT-LDA (red, full line), KPDF (blue, dashed), $\hat{\Pi}_{1,1/9}^0$ (black, dotted), and $\hat{\Pi}_{1,1}^0$ (green, dotted). Inset: exponential fall of the electronic tail outside the cluster.

Finally, the optical spectrum of the clusters is studied in a standard manner: the electrons are excited with a collective initial uniform velocity in the O_z direction. The dynamics under the effect of self-consistent fields is simulated, and the dipole moment $d(t) = \int n(\mathbf{r}, t) z d\mathbf{r}$ is computed. The optical spectrum is defined as $S(\omega) = \text{Im}d(\omega)$. The results are shown in Fig. 8. While all functionals provide good qualitative agreement with KS-LDA, the KPDF is able to predict the peak of the surface plasmon 10% more accurately than $\hat{\Pi}_{9/5,1}^0$. More importantly, the width of the peak, i.e., the Landau damping, is far better reproduced, given the damping term $\hat{\gamma}$ present in Eq. (15).

IV. CONCLUSIONS AND DISCUSSIONS

In the present work, a kinetic pressure density functional for a Fermi gas has been derived. The functional is designed to reproduce exactly the homogeneous equilibrium and the linear response in accordance with the kinetic/microscopic theories. It completely neglects temperature effects assuming $T = 0$ K and includes exchange-correlation effects only in an ad-hoc manner through the LDA effective potential (without the use of a proper xc field-factor [17]). While exact in principle, the functional poses a very difficult task due to its

space and, more importantly, time nonlocality. To solve this issue, an approximation of the functional has been proposed, reformulating the integral form into a wavelike equation, with the advantage of being local in time.

After spectral analysis, it is shown that the approximation is capable of resolving all asymptotic limits of the frequency-wavelength domain and interpolating fairly well the intermediate regions, i.e., the particle-hole continuum. In practice, for the Fermi gas, it is able to provide results that are one order of magnitude closer to the *exact* microscopic pressure, justifying the numerical effort compared to other existing functionals. Also, at least qualitatively, it is capable of going beyond linear regimes.

The main limitation of the approximation appears as an outcome of the constraints that tacitly assume the thermodynamic limit. Therefore, one of the important features of small, finite systems, namely the discreteness (the shell effect), cannot be reproduced. This problem is connected with a more subtle one, called the N -representability problem [47]. Nonetheless, the results provided by the KPDF are still superior to some other density functionals, also giving access to a better representation of dissipative processes, i.e., Landau damping.

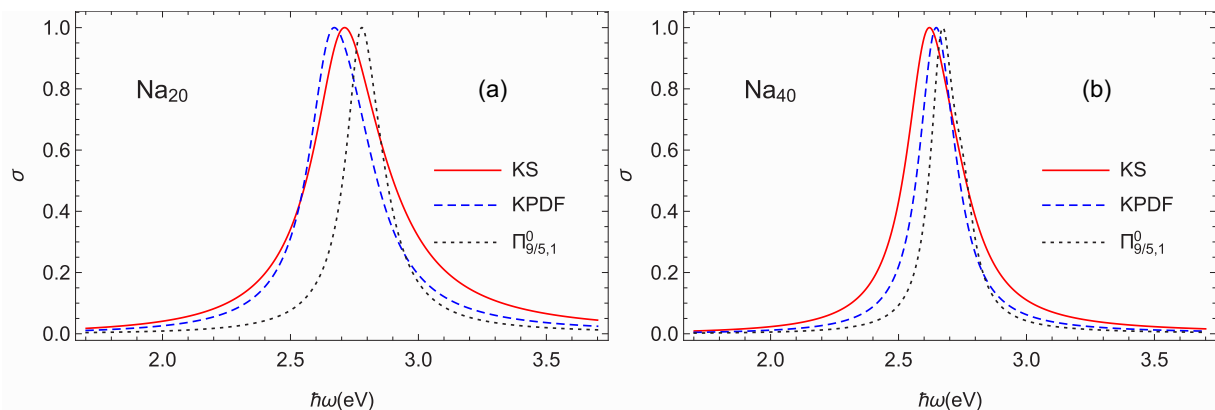


FIG. 8. Normalized optical cross-section spectrum for Na_{20} (left) and Na_{40} (right) cluster computed with KS (DFT-LDA) (red, full line), KPDF (blue, dashed), and $\hat{\Pi}_{9/5,1}^0$ (black, dotted).

The purpose of this work goes beyond designing a new functional within the orbital-free DFT. It entails creating a new path to a class of possible functionals. Apart from including other effects as spin, temperature, etc., one could systematically improve the present results in a number of ways. The next logical step would be to constrain the KPFD to reproduce the second-order linear-response function of a HFG. In this way, the decoupling ansatz used in the derivation would be removed, and also a better congruence with the nonlinear regime should be expected. Secondly, one might find simpler or better ways to remove the problem of time nonlocality and such to minimize the errors associated with the particle-hole continuum.

ACKNOWLEDGMENT

This work was partially supported by the Romanian Ministry of Research and Innovation by the contract PN 18 13 01 03.

APPENDIX

1. Pressure decomposition

One can start from the kinetic prescription of the total pressure,

$$\hat{\Pi}(\mathbf{r}, t) = -\frac{\hbar^2}{4m^2} \lim_{\mathbf{r}' \rightarrow \mathbf{r}} (\nabla_{\mathbf{r}} - \nabla_{\mathbf{r}'}) \otimes (\nabla_{\mathbf{r}} - \nabla_{\mathbf{r}'}) \rho(\mathbf{r}, \mathbf{r}', t),$$

and proceed in three steps. First, the collective velocity field is isolated by the transformation $\rho(\mathbf{r}, \mathbf{r}', t) \equiv e^{iS_0(\mathbf{r}, t)} \rho(\mathbf{r}, \mathbf{r}', t) e^{-iS_0(\mathbf{r}', t)}$ with $\nabla S_0 = m\mathbf{u}(\mathbf{r}, t)$, which gives

$$\hat{\Pi} = \frac{\mathbf{j} \otimes \mathbf{j}}{n} - \frac{\hbar^2}{4m^2} \lim_{\mathbf{r}' \rightarrow \mathbf{r}} (\nabla_{\mathbf{r}} - \nabla_{\mathbf{r}'}) \otimes (\nabla_{\mathbf{r}} - \nabla_{\mathbf{r}'}) \rho(\mathbf{r}, \mathbf{r}', t).$$

Then, together with the identity

$$\begin{aligned} & \lim_{\mathbf{r}' \rightarrow \mathbf{r}} (\nabla_{\mathbf{r}} - \nabla_{\mathbf{r}'}) \otimes (\nabla_{\mathbf{r}} - \nabla_{\mathbf{r}'}) \rho(\mathbf{r}, \mathbf{r}', t) \\ &= 2\nabla \otimes \nabla \rho - \lim_{\mathbf{r}' \rightarrow \mathbf{r}} (\nabla_{\mathbf{r}} \otimes \nabla_{\mathbf{r}'} + \nabla_{\mathbf{r}'} \otimes \nabla_{\mathbf{r}}) \rho(\mathbf{r}, \mathbf{r}', t), \end{aligned}$$

the transformation $\rho(\mathbf{r}, \mathbf{r}', t) \equiv n^{1/2}(\mathbf{r}, t) \tilde{\rho}(\mathbf{r}, \mathbf{r}', t) n^{1/2}(\mathbf{r}', t)$ is used to obtain

$$\begin{aligned} \hat{\Pi} &= \frac{\mathbf{j} \otimes \mathbf{j}}{n} + \hat{\Pi}_B[n] + \frac{\hbar^2}{2m^2} n \lim_{\mathbf{r}' \rightarrow \mathbf{r}} (\nabla_{\mathbf{r}} \otimes \nabla_{\mathbf{r}'} + \nabla_{\mathbf{r}'} \otimes \nabla_{\mathbf{r}}) \\ &\quad \times \tilde{\rho}(\mathbf{r}, \mathbf{r}', t). \end{aligned}$$

The final transformation is to isolate the TF-like density matrix $\rho_{\text{TF}} = 3nj_1(k_F|\mathbf{r} - \mathbf{r}'|)/(k_F|\mathbf{r} - \mathbf{r}'|)$ from $\tilde{\rho}$ to obtain

$$\begin{aligned} \hat{\Pi} &= \frac{\mathbf{j} \otimes \mathbf{j}}{n} + \hat{\Pi}_B[n] + \hat{\Pi}_{\text{TF}}[n] + \hat{\Pi}_{\text{NL}}[n], \\ \hat{\Pi}_{\text{NL}}[n] &= \frac{\hbar^2}{2m^2} n \lim_{\mathbf{r}' \rightarrow \mathbf{r}} (\nabla_{\mathbf{r}} \otimes \nabla_{\mathbf{r}'} + \nabla_{\mathbf{r}'} \otimes \nabla_{\mathbf{r}}) \tilde{\tilde{\rho}}(\mathbf{r}, \mathbf{r}', t). \end{aligned}$$

The nonlocal pressure is rearranged as in integral form over space-time with the nonlocal density-dependent kernel

$$\begin{aligned} \hat{\Pi}_{\text{NL}} &= \frac{\hbar^2}{2m^2} \int dx' \delta(x - x') (\nabla_{\mathbf{r}} \otimes \nabla_{\mathbf{r}'} \\ &\quad + \nabla_{\mathbf{r}'} \otimes \nabla_{\mathbf{r}}) \tilde{\rho}(x, x') \end{aligned}$$

$$\begin{aligned} \tilde{\rho}(x, x') &= \int dy dy' n^{1/2}(y) O(x, y, x', y'; n(x), \\ &\quad \times n(x')) n^{1/2}(y), \end{aligned}$$

where $x = (\mathbf{r}, t)$, $y = (\mathbf{r}', t')$.

While a supplementary dependency on density could be imposed as $O[x, y, x', y'; n(x), n(x'), n(y), n(y')]$, in practice, this would only make the functional harder to implement without any improvements. The time-space invariance of n_0 implies $O(x, y, x', y'; n_0, n_0) \equiv O(x - y, x' - y'; n_0, n_0)$, therefore a Fourier representation [$\xi = (\omega, k)$] of the kernel is chosen in order to apply the linear-response condition:

$$\begin{aligned} & O(x - y, x' - y'; n_1, n_2) \\ &= \int d\xi d\zeta e^{-i\xi(x-y)} \tilde{O}(\xi, \zeta; n_1, n_2) e^{-i\zeta(x'-y')}. \end{aligned}$$

The constraints (10) and (11) can be reformulated for the nonlocal pressure as

$$\Pi_{\text{NL}}[n_0] = 0,$$

$$\tilde{\mathfrak{F}} \left\{ \left(\frac{\delta \Pi_{\text{NL}}}{\delta n} \right)_{n_0} \right\} = \phi(\xi) = \frac{\omega^2}{k^2} - \frac{n_0}{m\chi(\omega, k)} - \frac{\delta \Pi_B}{\delta n} - \frac{\delta \Pi_{\text{TF}}}{\delta n},$$

which in terms of kernel \tilde{O} can be rewritten after some calculus as

$$\lim_{\substack{\xi_1 \rightarrow 0 \\ \xi_2 \rightarrow 0}} (\underline{\xi}_1 \otimes \underline{\xi}_2 + \underline{\xi}_2 \otimes \underline{\xi}_1) \tilde{O}(\xi_1, \xi_2; n_0, n_0) = 0,$$

$$\frac{\hbar^2}{m^2} \lim_{\substack{\xi_1 \rightarrow \xi \\ \xi_2 \rightarrow 0}} (\underline{\xi}_1 \otimes \underline{\xi}_2 + \underline{\xi}_2 \otimes \underline{\xi}_1) \tilde{O}(\xi_1, \xi_2; n_0, n_0) = \phi(\xi),$$

where $\underline{\xi} = \mathbf{k}$, the spatial components of the quadrivector ξ . A supplementary ansatz is used to remove the null behavior at the origin and decouple the integrals:

$$O(\xi, \zeta; n_1, n_2) \equiv \{O(\xi; n_1) + O(\zeta; n_2)\} / (\underline{\xi} \cdot \underline{\zeta}).$$

Using these in the formula for Π_{NL} , one gets

$$\hat{\Pi}_{\text{NL}}[n] = \int dx' \mathcal{L}(x, x') [n^{1/2}(x) \mathcal{D}(x') + n^{1/2}(x') \mathcal{D}(x)],$$

$$\mathcal{L}(x, x') = \delta(x - x') (\nabla_{\mathbf{r}} \otimes \nabla_{\mathbf{r}'} + \nabla_{\mathbf{r}'} \otimes \nabla_{\mathbf{r}}) (\nabla_{\mathbf{r}} \nabla_{\mathbf{r}'})^{-1},$$

$$\mathcal{D}(x) = \frac{1}{2} \int dy \int d\xi e^{-i\xi(x-y)} \phi(\xi; n(x)) n^{1/2}(y).$$

2. Approximating the kernel

The Drude model for the dielectric function is well known:

$$\varepsilon = 1 - \frac{\omega_p}{\omega^2 + i\omega\gamma}.$$

Since the dielectric function is related to the LRF, and implicitly to the kernel ϕ by $\varepsilon = 1 - v(k)\chi(\omega, k)$, the following approximative form is proposed:

$$\phi^{\text{app}}(w, q) \approx \phi_0^\infty \frac{w^2 - i\gamma(q)w + t_2(q)}{w^2 - i\gamma(q)w + t_1(q)},$$

where the scaled spectral variables $w = \hbar^2 k_F^2 / (2m\omega)$, $q = k/k_F$ have been used. This approximation is designed to

express the w dependency as a rational function and to reproduce *simultaneously* the asymptotic limits $\omega = 0$, $\omega \rightarrow \infty$ as well as the midline within the particle-hole continuum $w = q^2 + q$. Rewriting the convolution expression for \mathcal{D} as $\mathcal{D} = \phi^{\text{app}} \otimes n^{1/2}$, applying the Fourier transform, rearranging the terms, and applying an inverse Fourier transform, one can write down a wave equation for \mathcal{D} :

$$[\partial_{t,t} - \hat{\gamma} \partial_t - \hat{t}_1] \mathcal{D} = \frac{4}{15} k_F^2 [\partial_{t,t} - \hat{\gamma} \partial_t - \hat{t}_2] n^{1/2}, \quad (\text{A1})$$

where, through the LDA limit for 3D systems, $k_F = (3\pi^2 n)^{1/3}$ and the spatial operators γ, t_1, t_2 are

applied in accordance with the above Fourier prescription as

$$\hat{\gamma} f(\mathbf{r}) = \int d\mathbf{r}' \left[\int d\mathbf{k} e^{i\mathbf{k}(\mathbf{r}-\mathbf{r}')} \gamma \left(\frac{\mathbf{k}}{k_F(\mathbf{r})} \right) \right] f(\mathbf{r}').$$

The functions $\gamma, t_1, t_2, \phi_0^0, \phi_1^\infty$ are defined analytically through the hierarchy:

$$\begin{aligned} \Psi_3(z) &= \frac{1}{4} (1 - z^2) \log \left(\frac{z+1}{z-1} \right) + \frac{z}{2}, & \tilde{\chi}(w, q) &= \frac{3[\Psi_3(\frac{w}{2q} - \frac{q}{2}) - \Psi_3(\frac{w}{2q} + \frac{q}{2})]}{q}, \\ \phi(w, q) &= \frac{w^2}{4q^2} - \frac{q^2}{4} - \frac{1}{3} - \frac{1}{\tilde{\chi}(w, q)}, & \lim_{w \rightarrow \infty} \phi(w, z) &= \phi_0^\infty + \phi_1^\infty(q)/w^2, & \phi_1^\infty(q) &= \frac{4q^4}{5} + \frac{48q^2}{175}, & \phi_0^\infty &= \frac{4}{15}, \\ \phi_0^0(q) &= \phi(0, q), & t_1(q) &= \frac{\phi_1^\infty(q)}{\phi_0^0(q) - \phi_0^\infty}, & t_2(q) &= t_1(q) \frac{\phi_0^0(q)}{\phi_0^\infty}, & \phi_0^0(q) &\equiv \phi(\omega = 0, q), \\ \gamma(q) &= \frac{-i}{q^2 + q} \left((q^2 + q)^2 + \phi_1^\infty(q) \frac{\phi_0^0(q) - \phi(q^2 + q, q)}{[\phi_0^0(q) - \phi_0^\infty][\phi(q^2 + q, q) - \phi_0^\infty]} \right). \end{aligned}$$

We note that, in the limit of small spatial oscillations $|\nabla \ln n| \ll k_F$,

$$\begin{aligned} \hat{\gamma} f(\mathbf{r}) &\approx \frac{0.87 - 0.5i}{k_F} |\nabla| f(\mathbf{r}) + \frac{0.28 + 0.5i}{k_F^2} \nabla^2 f(\mathbf{r}), \\ \hat{t}_2 f(\mathbf{r}) &\approx \frac{6}{7k_F^4} \nabla^4 f(\mathbf{r}), \\ \hat{t}_1 f(\mathbf{r}) &\approx \frac{36}{35k_F^2} \nabla^2 f(\mathbf{r}) - \frac{15}{7k_F^4} \nabla^4 f(\mathbf{r}). \end{aligned}$$

-
- [1] L. B. Fletcher, H. J. Lee, T. Döppner, E. Galtier, B. Nagler, P. Heimann, C. Fortmann, S. LePape, T. Ma, M. Millot *et al.*, *Nat. Photon.* **9**, 274 (2015).
- [2] J. A. Scholl, A. L. Koh, and J. A. Dionne, *Nature (London)* **483**, 421 (2012).
- [3] F. Calvayrac, P.-G. Reinhard, E. Suraud, and C. Ullrich, *Phys. Rep.* **337**, 493 (2000).
- [4] N. Crouseilles, P.-A. Hervieux, and G. Manfredi, *Phys. Rev. B* **78**, 155412 (2008).
- [5] J. J. Fortney, *Contrib. Plasma Phys.* **53**, 385 (2013).
- [6] M. S. Tame, K. R. McEnery, S. K. Özdemir, J. Lee, S. A. Maier, and M. S. Kim, *Nat. Phys.* **9**, 329 (2013).
- [7] J. A. Schuller, E. S. Barnard, W. Cai, Y. C. Jun, J. S. White, and M. L. Brongersma, *Nat. Mater.* **9**, 193 (2010).
- [8] D. K. Gramotnev and S. I. Bozhevolnyi, *Nat. Photon.* **4**, 83 (2010).
- [9] N. L. Tsintsadze and L. N. Tsintsadze, *Europhys. Lett.* **88**, 35001 (2009).
- [10] F. Haas, M. Marklund, G. Brodin, and J. Zamanian, *Phys. Lett. A* **374**, 481 (2010).
- [11] R. McWeeny, *Methods of Molecular Quantum Mechanics* (Academic, London, UK, 1992).
- [12] E. Runge and E. K. U. Gross, *Phys. Rev. Lett.* **52**, 997 (1984).
- [13] C. Gardner, *SIAM J. Appl. Math.* **54**, 409 (1994).
- [14] A. Domsps, P.-G. Reinhard, and E. Suraud, *Phys. Rev. Lett.* **80**, 5520 (1998).
- [15] D. Michta, F. Graziani, and M. Bonitz, *Contrib. Plasma Phys.* **55**, 437 (2015).
- [16] D. I. Palade and V. Baran, *J. Phys. B* **48**, 185102 (2015).
- [17] Z. A. Moldabekov, M. Bonitz, and T. S. Ramazanov, *Phys. Plasmas* **25**, 031903 (2018).
- [18] G. Manfredi and F. Haas, *Phys. Rev. B* **64**, 075316 (2001).
- [19] W. Myers and W. Swiatecki, *Nucl. Phys. A* **601**, 141 (1996).
- [20] Y. Chu, B. Jennings, and M. Brack, *Phys. Lett. B* **68**, 407 (1977).
- [21] J. Clerouin, E. L. Pollock, and G. Zerah, *Phys. Rev. A* **46**, 5130 (1992).
- [22] P. K. Shukla and B. Eliasson, *Rev. Mod. Phys.* **83**, 885 (2011).
- [23] D. I. Palade, *Phys. Plasmas* **23**, 074504 (2016).
- [24] V. Karasiev and S. Trickey, *Comput. Phys. Commun.* **183**, 2519 (2012).
- [25] R. Benguria, H. Brezis, and E. H. Lieb, *Commun. Math. Phys.* **79**, 167 (1981).
- [26] D. Bohm, *Phys. Rev.* **85**, 166 (1952).
- [27] D. A. Kirzhnits, *Sov. Phys. JETP* **5**, 64 (1957).

- [28] V. V. Karasiev, D. Chakraborty, O. A. Shukruto, and S. B. Trickey, *Phys. Rev. B* **88**, 161108 (2013).
- [29] W. Yan, *Phys. Rev. B* **91**, 115416 (2015).
- [30] C. Ciraci and F. Della Sala, *Phys. Rev. B* **93**, 205405 (2016).
- [31] M. Akbari-Moghanjoughi, *Phys. Plasmas* **22**, 022103 (2015).
- [32] P. K. Shukla and B. Eliasson, *Phys. Rev. Lett.* **96**, 245001 (2006).
- [33] D. Shaikh and P. K. Shukla, *Phys. Rev. Lett.* **99**, 125002 (2007).
- [34] Y. A. Wang, N. Govind, and E. A. Carter, *Phys. Rev. B* **60**, 16350 (1999).
- [35] C. Huang and E. A. Carter, *Phys. Rev. B* **81**, 045206 (2010).
- [36] Z. Moldabekov, M. Bonitz, and T. Ramazanov, *Contrib. Plasma Phys.* **57**, 499 (2017).
- [37] J. Tao, X. Gao, G. Vignale, and I. V. Tokatly, *Phys. Rev. Lett.* **103**, 086401 (2009).
- [38] X. Gao, J. Tao, G. Vignale, and I. V. Tokatly, *Phys. Rev. B* **81**, 195106 (2010).
- [39] I. Tokatly and O. Pankratov, *Phys. Rev. B* **60**, 15550 (1999).
- [40] I. V. Tokatly and O. Pankratov, *Phys. Rev. B* **62**, 2759 (2000).
- [41] C. Ciraci, *Phys. Rev. B* **95**, 245434 (2017).
- [42] P. Hohenberg and W. Kohn, *Phys. Rev.* **136**, B864 (1964).
- [43] M. Bonitz, *Quantum Kinetic Theory* (B.G. Teubner, Leipzig, 2015).
- [44] D. Bohm and J. P. Vigier, *Phys. Rev.* **96**, 208 (1954).
- [45] G. Giuliani and G. Vignale, *Quantum Theory of the Electron Liquid* (Cambridge University Press, Cambridge, 2008).
- [46] D. Gottlieb and S. A. Orszag, *Numerical Analysis of Spectral Methods: Theory and Applications (CBMS-NSF Regional Conference Series in Applied Mathematics)* (Society for Industrial and Applied Mathematics, Philadelphia, PA, 1987).
- [47] M. Levy, *Proc. Natl. Acad. Sci. USA* **76**, 6062 (1979).
- [48] M. Brack, *Rev. Mod. Phys.* **65**, 677 (1993).
- [49] L. Hedin and B. I. Lundqvist, *J. Phys. C* **4**, 2064 (1971).